Electronic Supplementary Material (ESI) for Dalton Transactions.

SUPPORTING INFORMATION

Regulating the charge carrier transport rate via bridging ternary heterojunctions to enable CdS nanorods' solar-driven hydrogen evolution

Pooja Varma [a], Anjana E Sudheer [a], Assa Aravindh Sasikala Devi [b], D. Murali [a], D. Amaranatha Reddy [a*]

[a] *Department of Sciences, Indian Institute of Information Technology Design and Manufacturing, Kurnool-518007, Andhra Pradesh, India*

[b] *Nano and Molecular Systems Research Unit, University of Oulu, Pentti Kaiteran katu 1, 90570 Oulu, Finland*

** Corresponding author E-mail: drreddy@iiitk.ac.in (D.A.R.)*

1. Experimental Section

1.1 Synthesis of SnS_2 nanosheets:

SnS_2 nanosheets were synthesized through a simple hydrothermal method. Briefly, 1.056 g of $SnCl_4 \cdot 5H_2O$ and 1.086g of TAA were dispersed in 50 mL of DI water and stirred it for 40 min. The aforementioned combination was put into a 100 mL Teflon-lined stainless steel autoclave and kept at 160 °C for 12 hours in an electric hot air oven. After completion of the reaction, the autoclave was air-cooled to room temperature. A dark yellow precipitate was obtained and washed with ethanol and DI water three times and finally dried in an oven at 60°C for 8 h.

1.2 Synthesis of WS_2 nanosheets:

To synthesize WS_2 nanosheets, 2.5 g of WCl_6 and 5.0 g TAA were dissolved in 60 mL of deionized water and vigorously stirred for 1 h for complete dissolution of the mixture. Then the mixed solution was transferred to a 100 mL Teflon-lined stainless-steel autoclave and kept it for 24 h at 200°C. The mixture was spontaneously cooled to room temperature after the reaction.. Finally, the obtained black precipitate was collected and washed several times with ethanol and DI water to remove the contaminants and dried at 60 °C for 24 h.

1.3 Synthesis of SnS_2/WS_2 nanocomposites:

SnS_2/WS_2 nanocomposites were synthesized via solvent exfoliation method. Different wt. % of the above prepared bulk SnS_2 nanosheets and WS_2 were added to 10 mL of DMF and sonicated for 4 h. Later the obtained mixture was kept for magnetic stirring for about 12 h for efficient formation of hetero structures between SnS_2 and WS_2 nanostructures. Finally, a black precipitate was washed with ethanol and DI water till the solvent was removed. The product was then kept for drying at 80°C for 10h.

1.4 Synthesis of CdS nanorods:

CdS nanostructures were synthesized using facile solvothermal method using 4.62 g of Cd $(CH_3COO)_2.2H_2O$ and CH_4N_2S as a Cd and S source materials. Desired amount of above precursors was dissolved in 60 mL of EDA and vigorously stirred for 1 h using a magnetic stirrer. Next the above mixture was poured into a 100 mL Teflon-lined stainless-steel autoclave and kept it for 48h at 160°C. After the solvothermal reaction naturally cooled to room temperature. The final yellow colored precipitate was collected and then washed several times with ethanol and deionized water (DI) to remove the unwanted impurities. The obtained final product was kept for drying at 60 °C for 12h and use it for further photocatalytic application.

1.5 Synthesis of CdS/SnS_2 nanocomposites:

To synthesize CdS/SnS_2 nanocomposites, we followed the solvent exfoliation method in DMF via ultrasonication. The desired wt. % of bulk SnS_2 (2, 4, 6, 8, 10 wt %) is dispersed in 10 mL DMF and ultrasonicate for 2 h to obtain a few layered ultrathin 2D nanosheets. Accordingly, desired amount of CdS nanorods were added and continued the ultrasonication for the next 1 h. The mixed solution was subjected to magnetic stirring for 12 h to deposit SnS_2 ultrathin nanosheets onto the CdS nanorods and hence achieved the interfacial contact between bare CdS and SnS_2 nanostructures. Finally, the prepared samples were collected and washed several times with ethanol and DI water for the complete removal of the solvent. The product obtained was dried at 100°C for 8 h.

1.6 Synthesis of CdS/WS_2 nanocomposites:

To obtain the CdS/WS_2 nanocomposites, the bulk WS_2 is subjected to the solvent exfoliation method in DMF through ultrasonication. Different wt. % of bulk WS_2 (2, 4, 6, 8, 10

wt. %) was dispersed in 10 mL of DMF solution and ultrasonicated for 2 h to obtain a few layered ultrathin 2D WS_2 nanosheets. Subsequently, desired amount of CdS nanorods were added and continued the ultrasonication for the next 1 h. The mixed solution was then stirred for another 12 h to deposit WS_2 ultrathin nanosheets onto the CdS nanorods. After stirring, the prepared sample was collected and washed several times with ethanol and DI water for the complete removal of the impurities. The product was then subjected to heating at 100°C for 8 h.

1.7 Synthesis of CdS/SnS_2-WS_2 nanocomposites:

CdS/SnS_2-WS_2 nanocomposites were prepared through exfoliation method different wt. % of the bulk SnS_2 and WS_2 were added to 10 mL of DMF. First SnS_2 is ultrasonicated for 2 h to achieve the ultrathin nanosheets. Later, WS_2 is added to the exfoliated SnS_2 and sonicated for another 2 h. A black solution was formed into which CdS nanorods were added and continued the ultrasonication for the next 1 h. The mixed solution was subjected to magnetic stirring for 12 h to deposit SnS_2-WS_2 ultrathin nanosheets onto the CdS nanorods. After completion of the reaction, the prepared samples were collected and washed several times with ethanol and DI water. The product was then subjected to heating at 100°C for 10 h. The fabrication process of CdS/SnS_2-WS_2 is schematically represented in the Scheme I.

2. Characterization Techniques

Structural properties of the above synthesized nanostructures were analysed using Bruker D8 ADVANCE diffractometer with Cu Kα radiation. The X-ray photoelectron spectroscopy (XPS) was carried out using Al Kα radiation (1486.6 eV) with an energy of 15 kV/150 W. To obtain the details of microstructures of the photocatalysts, Transmission electron microscopy (TEM) and high-resolution TEM (HRTEM) were executed using JEOL JEM-2100F operated at an acceleration voltage of 200 kV. The atomic force microscopy (AFM) images were obtained by using a Multimode Nanoscope (Veeco, USA). The determination of the optical properties of the as-synthesized nanocomposite were performed using Diffuse reflectance spectra and photoluminescence (PL) spectra and were recorded with a UV-1800 SHIMADZU, and a Hitachi F-7000 fluorescence spectrometer respectively.

2.1 Photocatalytic measurements

The photocatalytic H_2 evolution experiments were carried out in a quartz reactor with 150 mL capacity, into which a solution of 15 mL of water, 3 mL of sacrificial agent (lactic acid), and 1 mg of synthesized photocatalysts were added. The reactor was closed tightly with an air tight rubber septum. A solar simulator with an AM 1.5 G filter was employed as the light source. The light intensity was adjusted to 1 sun (100 mW/cm^2) using a Si reference cell. Before start the light irradiation, the system was evacuated for 30 min and degasified with Argon for 30 min for the complete removal of air in the system. The assessment of H_2 generation was conducted by an offline gas chromatograph provided with a thermal conductivity detector. The apparent quantum efficiency (AQE) of the prepared nanostructures for H_2 can be calculated using the following equation:

$$\text{Quantum yield} = \frac{\text{number of reacted electrons}}{\text{number of incident photons}} \times 100\%$$

$$= 2 \times \frac{\text{number of evolved H2 molecules}}{\text{number of incident photons}} \times 100\%$$

2.2 Photo-electrochemical measurements

Photo-electrochemical measurements were carried out in a three-electrode system using a Biologic electrochemical workstation. Solar simulator equipped with an AM 1.5G filter was used as a light source. The output light intensity was adjusted to 1 sun (100 W/m^2) using 15151 low-cost calibrated Si reference cell. Ag/AgCl and platinum wire, were used as the reference and counter electrodes respectively, and 0.5 M Na_2SO_4 aqueous solution served as the electrolyte. The measured pH value of electrolyte solution is 6.72. To prepare the working electrode, the as-synthesized 10 mg of CdS, CdS/WS_2, CdS/SnS_2 and CdS/SnS_2-WS_2 nanocomposites were first dispersed into ethanol (450 µl) and 50 µl Nafion mixtures using soft ultrasonic stirring to obtain a uniform suspension. The solution containing the catalyst (30 µl) was dropped onto the indium– tin oxide (ITO) conductor glass substrate, which was then dried in an oven at 80 °C for 3 h. Photoresponses were measured at 0.0 V during on-off cycling of the solar simulator. Electrochemical impedance spectroscopy (EIS) was carried out at open-circuit potential over the frequency range of 105 and 10^{-1} Hz with an AC voltage magnitude of 5 mV. Moreover, to evaluate the flat-band potential (VFB) of the CdS, SnS_2, WS_2, and SnS_2-WS_2 Mott−Schottky plots at a frequency of 1 kHz were measured using a standard potentiostat equipped with an impedance spectra analyzer in the same electrochemical configuration and electrolyte under the dark condition. The measured potentials versus Ag/AgCl were converted to the normal hydrogen electrode (NHE) scale by $E_{NHE} = E_{Ag/AgCl} + 0.197$ at pH=7

3. Computational Methodology

The theoretical calculations were performed using Vienna Ab initio Simulation Package (VASP) with projector augmented wave (PAW) method with plane-wave basis. It was implemented via generalization-gradient approximation (GGA) with exchange–correlation function of Perdew-Burke-Ernzerhof (PBE) [S1]. Since PBE functional underestimate bandgaps, HSE06 functional were used to correctly reproduce experimental bandgaps [S2]. For Brillouin zone sampling, a tight 16x16x1 k-grid and 16x16x16 k-grid were used for SnS2, WS2 and CdS systems. The plane wave cut-off energy was chosen as 650 eV. Along with strict energy and force convergence during full relaxation, convergence was checked with respect to vacuum layers as well. The lattice parameters and bandgap values show good agreement with reported theoretical and experimental values.

In order to model HER reaction, 4X4X1 supercells of WS2 & SnS2 and nanowire of CdS were constructed with appropriate k-points. For the calculation of H adsorption energy, Single H atom was placed on top of S atom of WS2, SnS2 surface. H atom was placed on S atom of CdS nanowire. HER reaction proceeds in two steps and the adsorption energy of H is the rate determining step. We followed the methodology proposed by Norskov [S3] in order to calculate HER reaction in CdS, WS_2 and SnS_2 surfaces. The energetics is given in table S1.

4. Supporting Figures

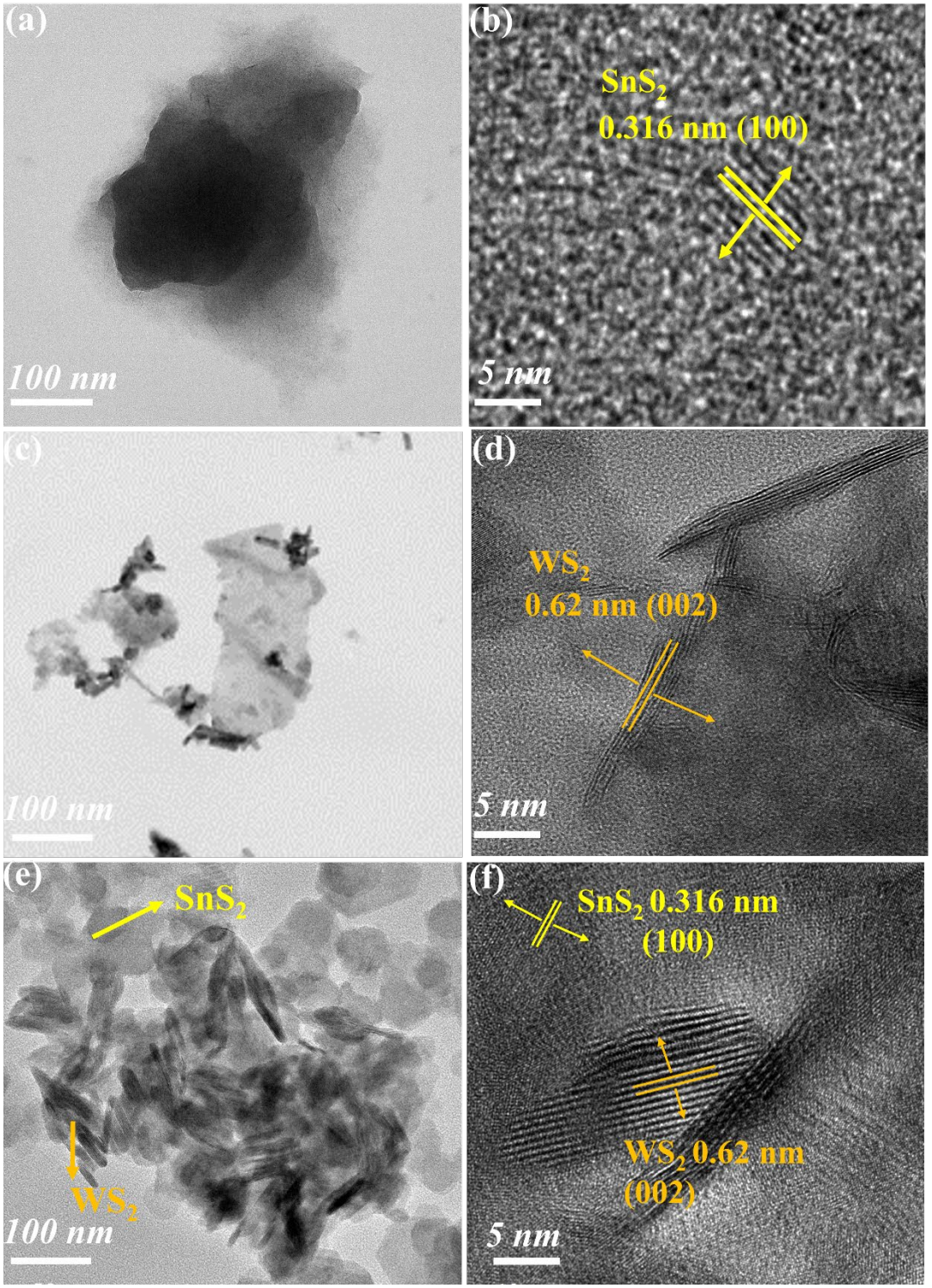

Figure S1: FETEM and HRTEM micrographs of (a, b) SnS_2 nanostructures, (c, d) WS_2 nanostructures, (e, f) SnS_2-WS_2 nanostructures.

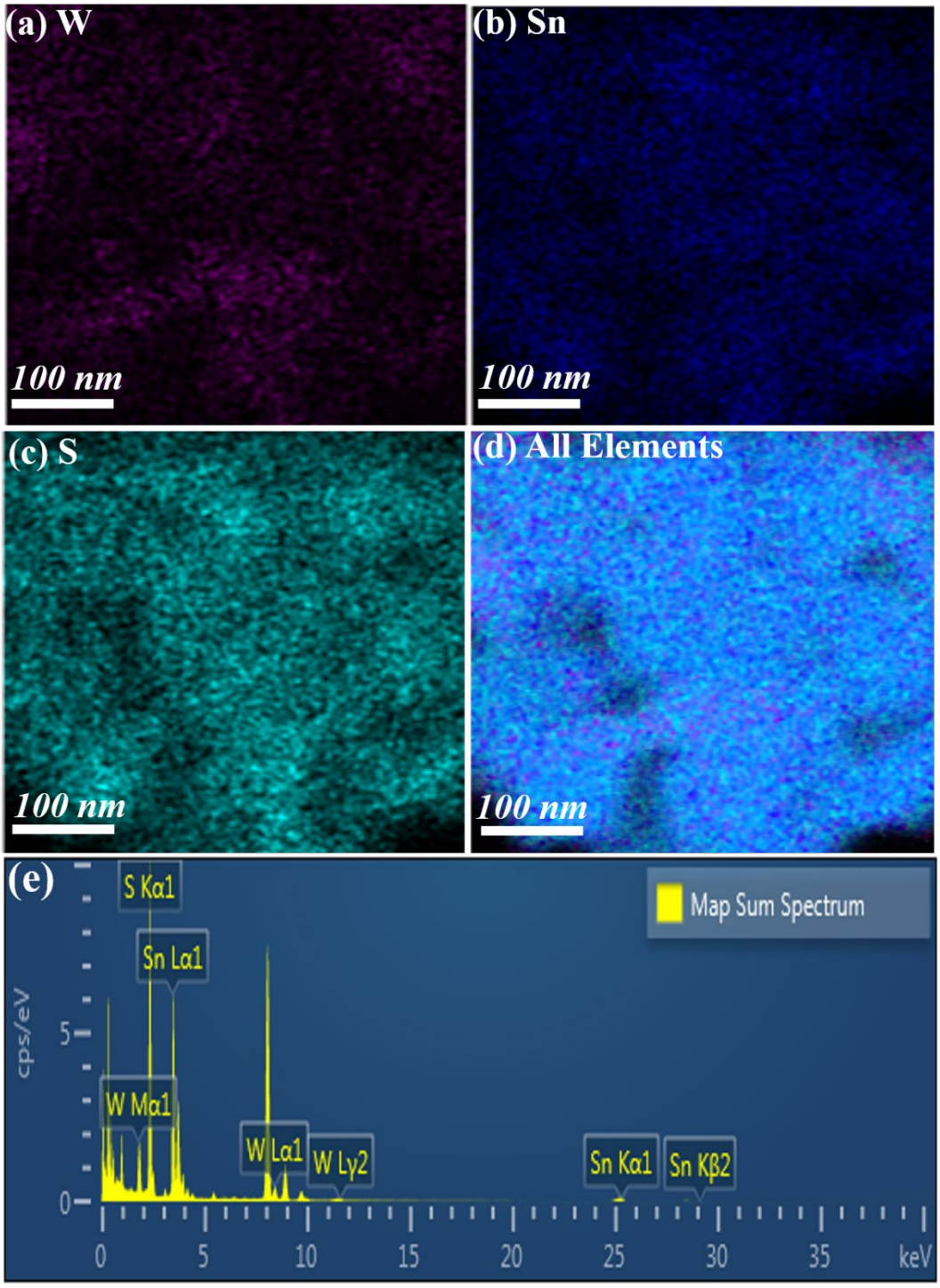

Figure S2: (a-d) EDS mapping micrographs of SnS_2-WS_2 nanostructures. (e) Line spectra of SnS_2-WS_2 nanostructures.

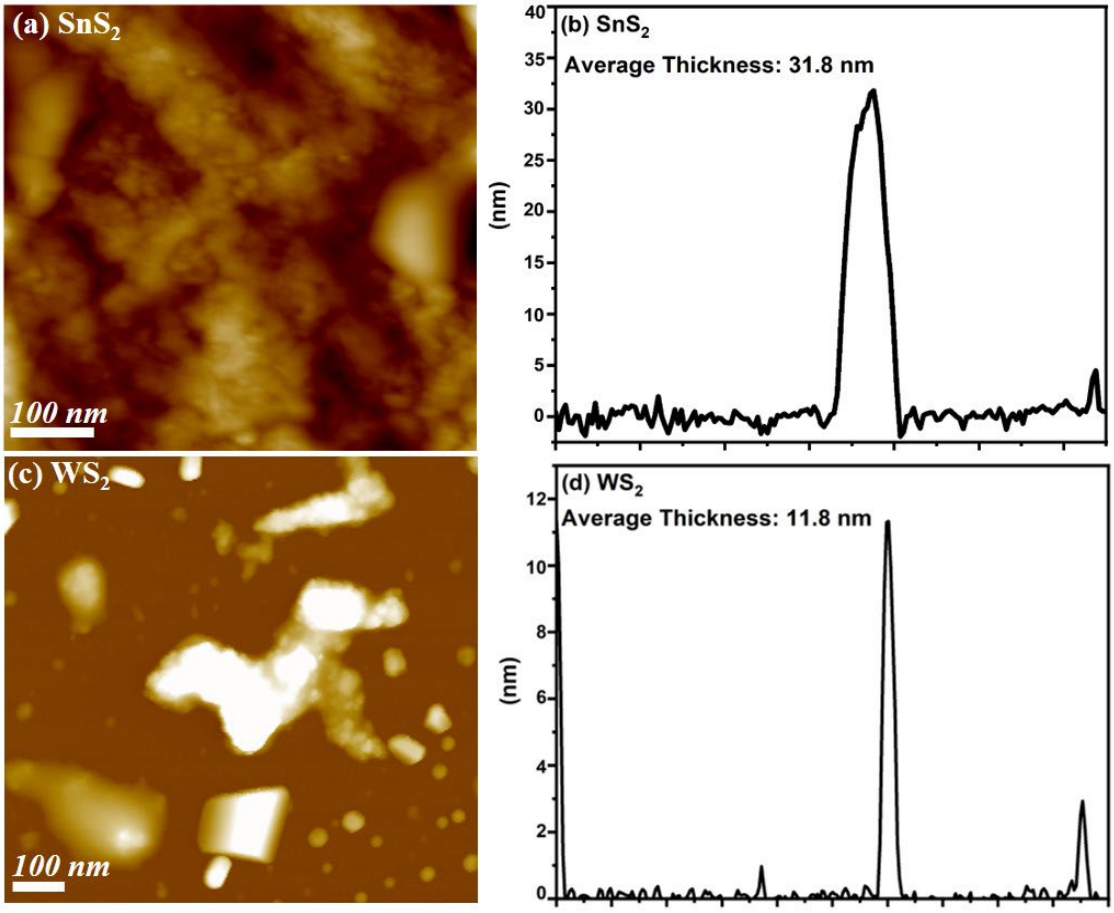

Figure S3: AFM image and corresponding thickness of **(a, b)** SnS_2 nanosheets and **(c, d)** WS_2 nanosheet.

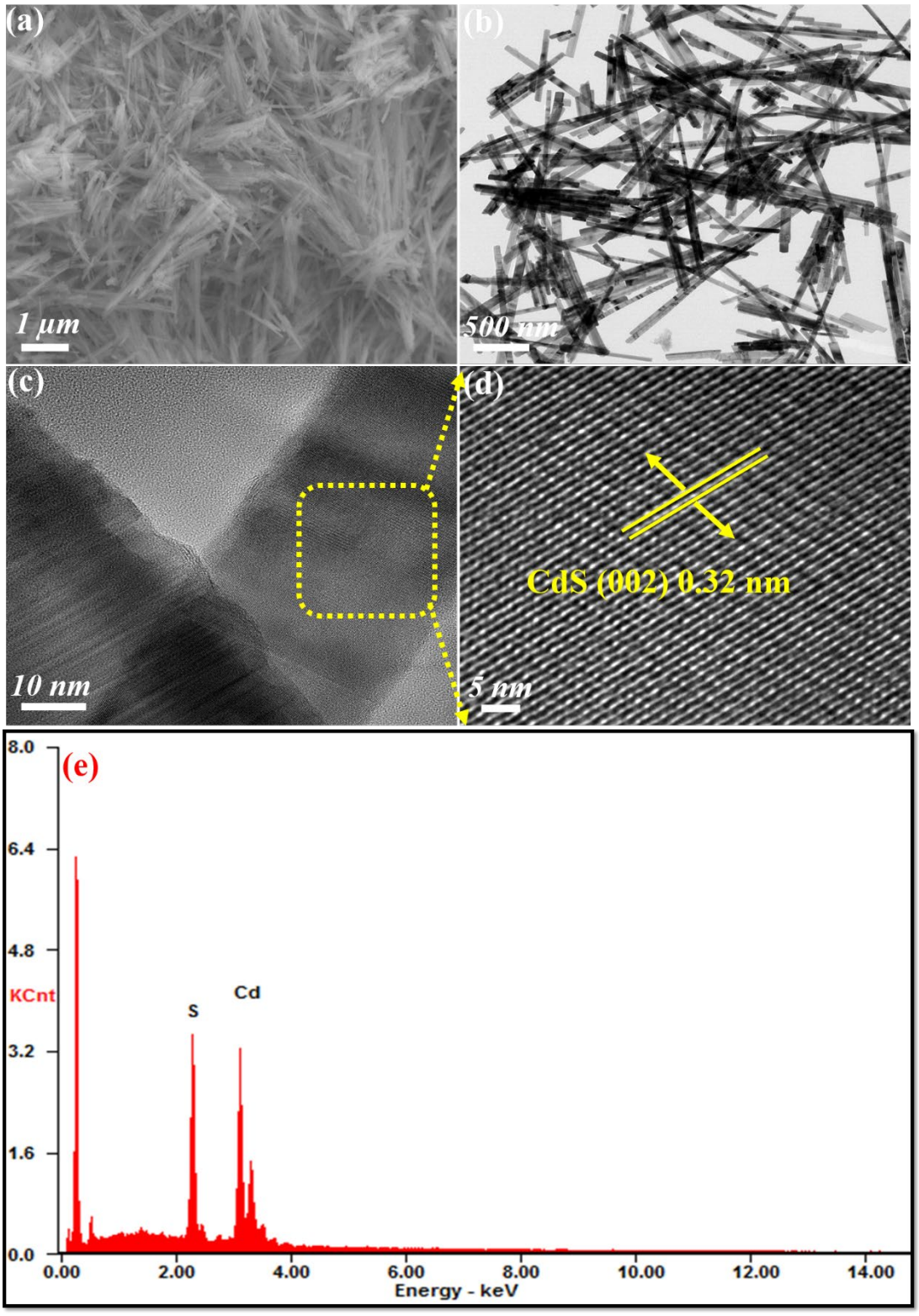

Figure S4: (a) FESEM micrograph of as prepared CdS nanorods. (b-d) Corresponding FETEM and HRTEM images of CdS nanorods respectively. (e) EDS line spectra of CdS nanorods.

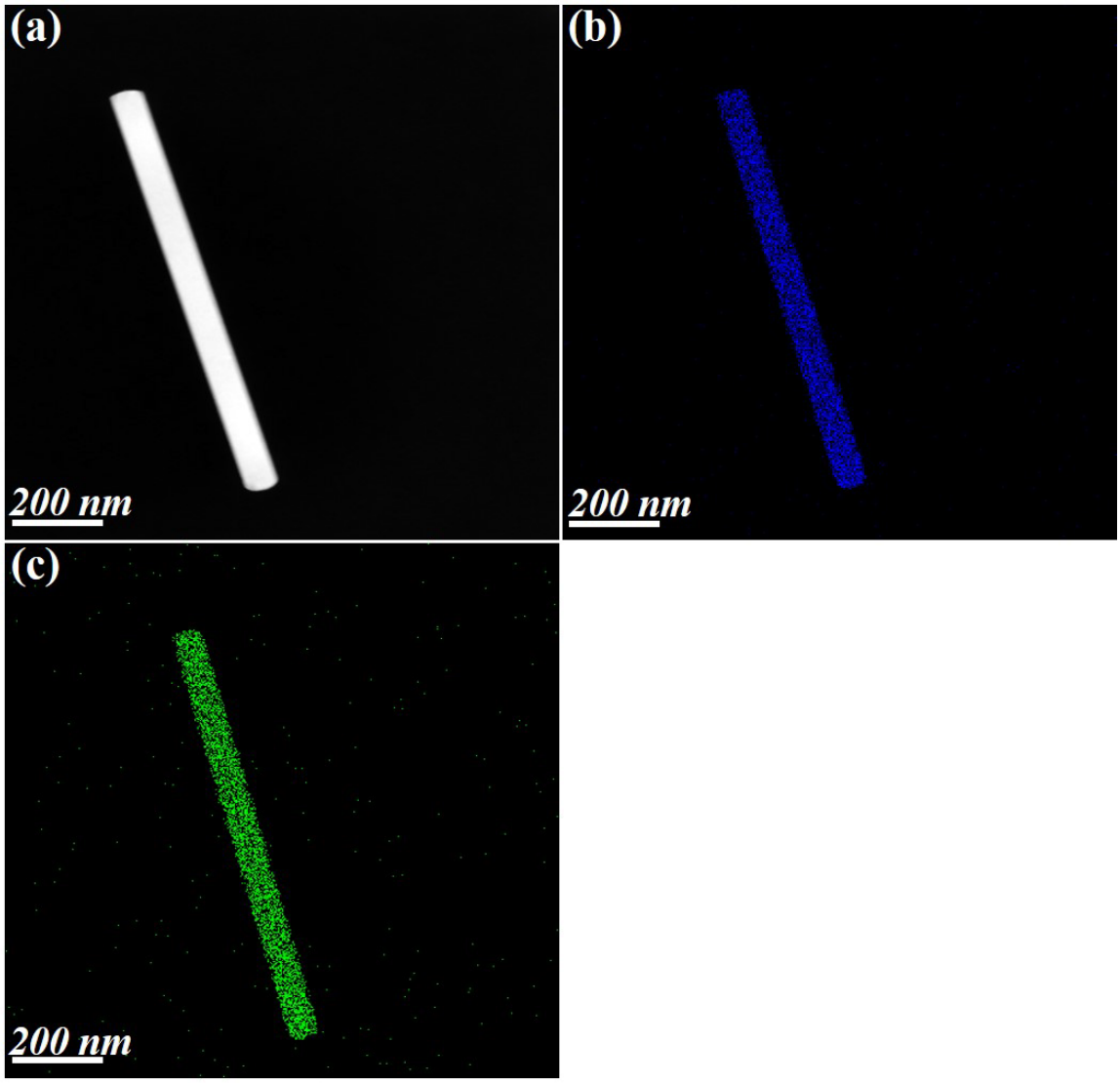

Figure S5: EDS mapping micrographs of CdS nanorods (a) Electron Image (b) Cd (c) S elements respectively.

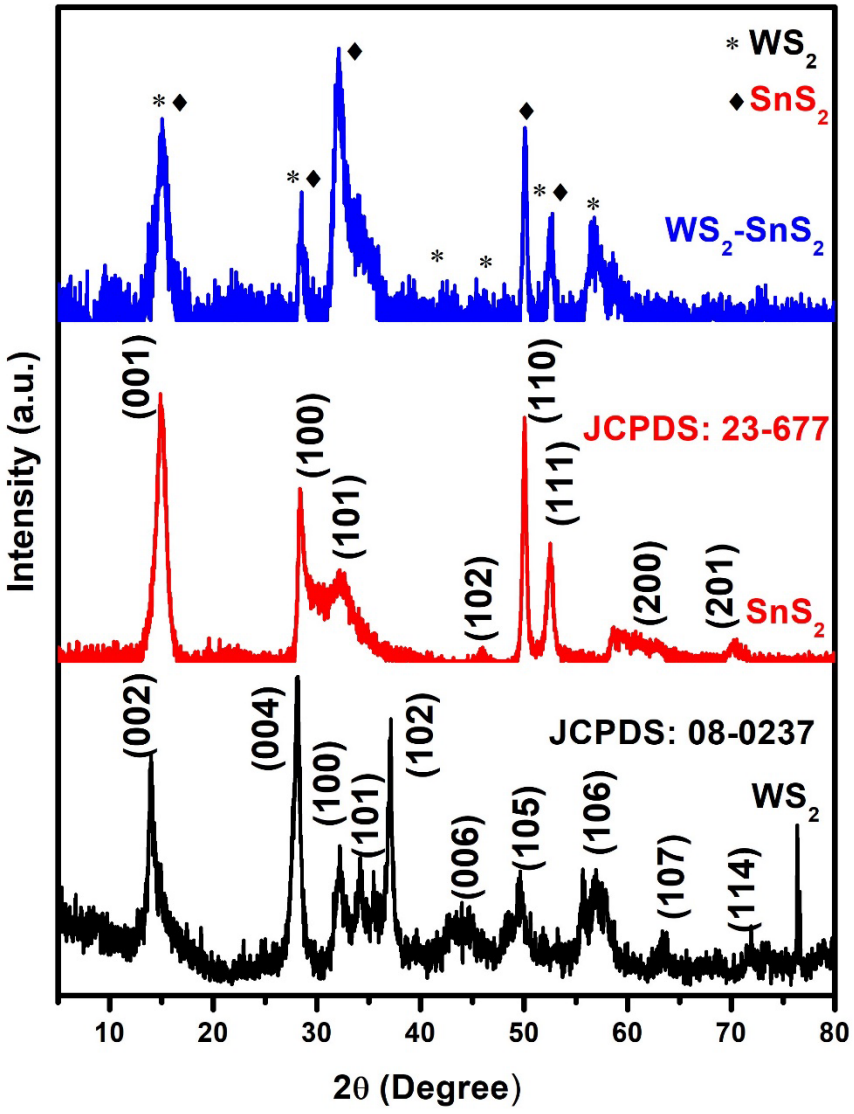

Figure S6: XRD patterns of the WS_2, SnS_2 and WS_2-SnS_2 nanostructures.

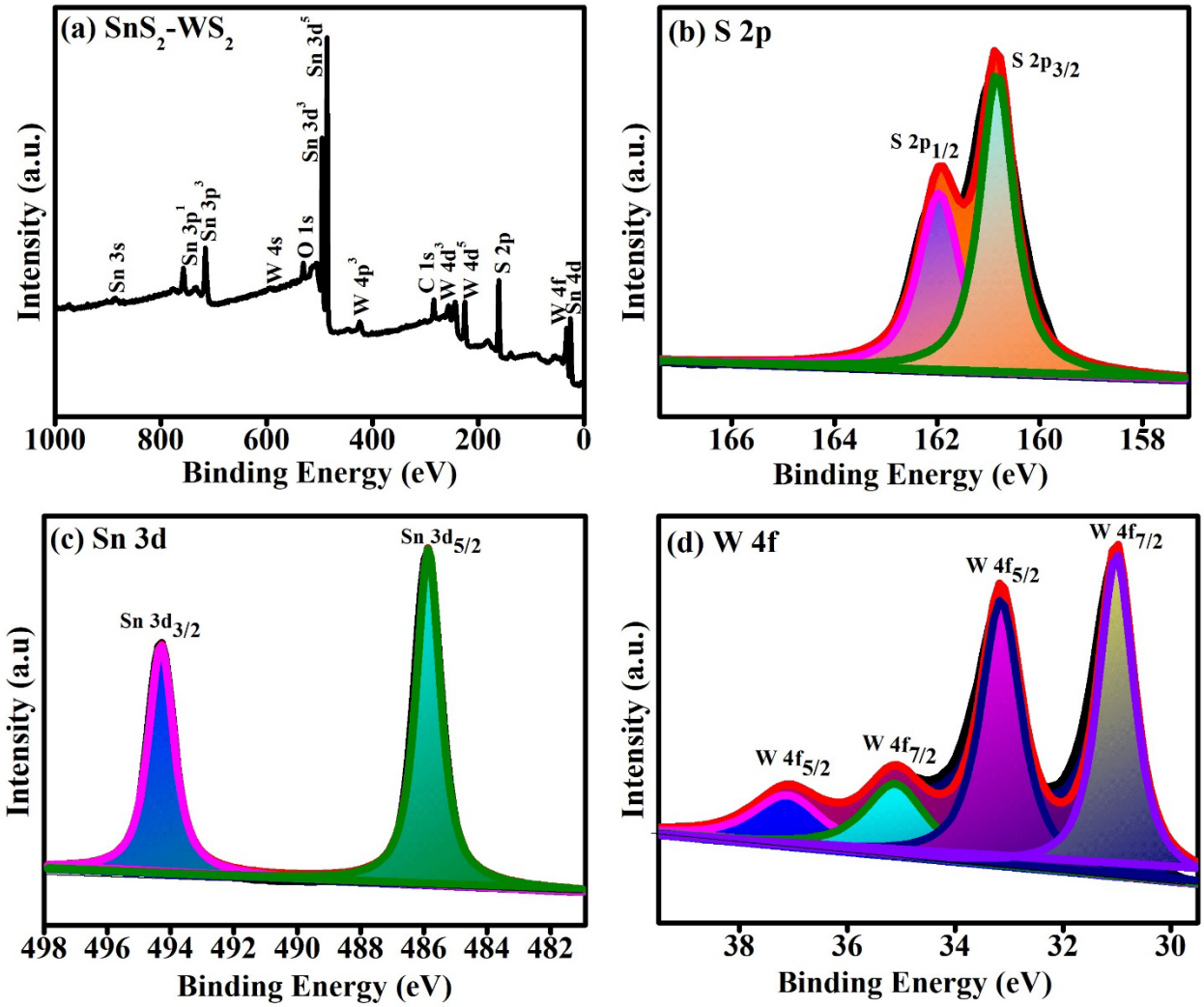

Figure S7: (a) XPS survey spectrum of SnS_2-WS_2 nanostructures. (b-d) Corresponding core level XPS spectra of S 2p, Sn 3d and W 4f respectively.

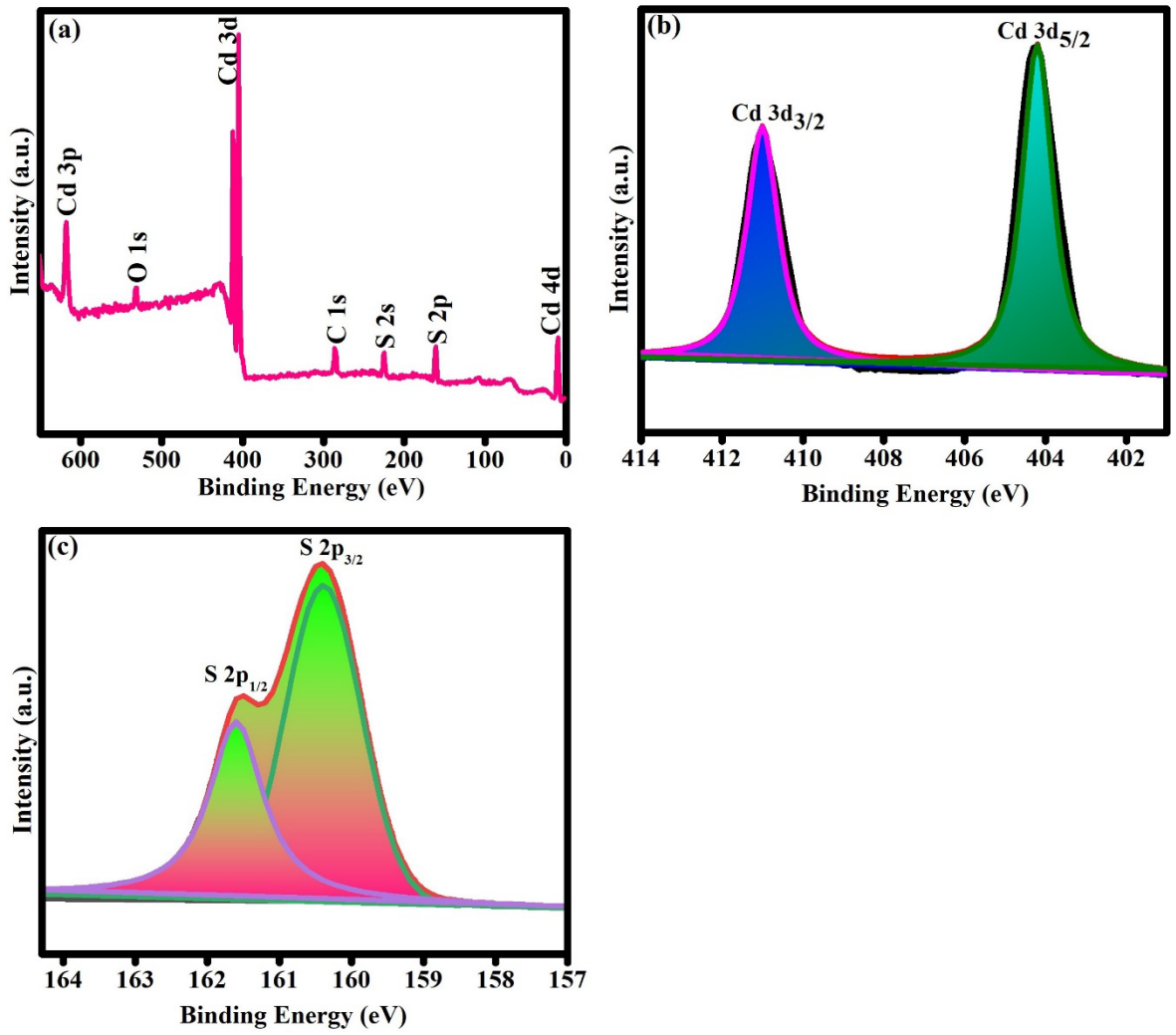

Figure S8: (a) XPS survey spectrum of CdS nanorod. (b, c) Corresponding core level XPS spectra of Cd 3d and S 2p respectively.

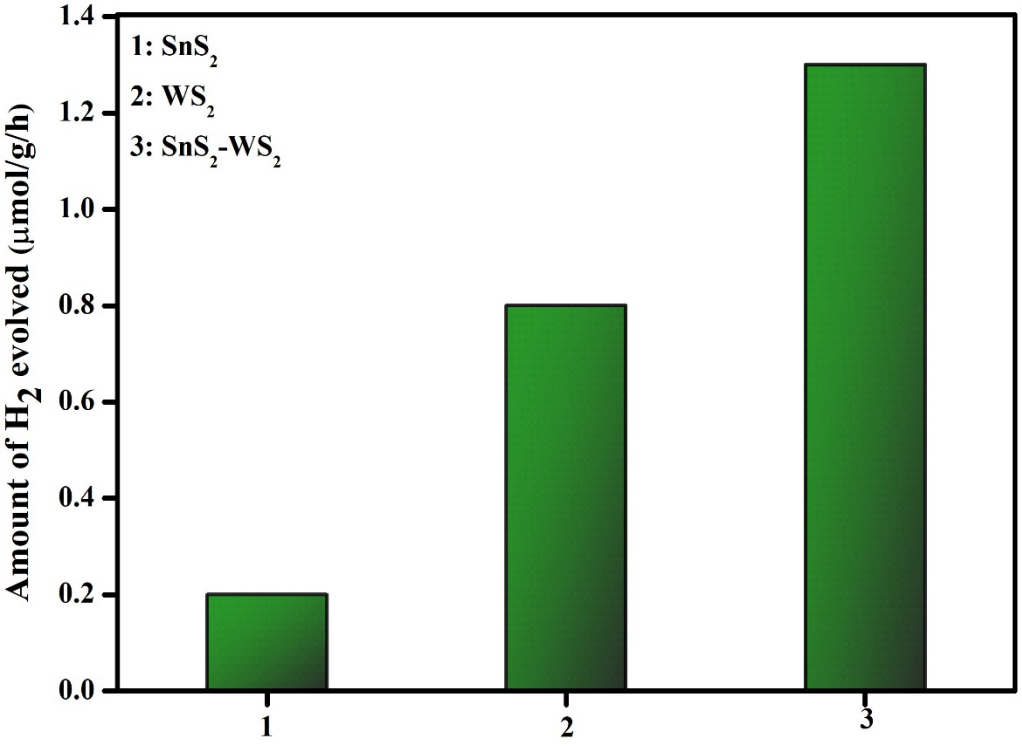

Figure S9: Amount of hydrogen evolved under sunlight irradiation using SnS_2, WS_2 and SnS_2-WS_2 nanostructures as a photo catalysts, respectively.

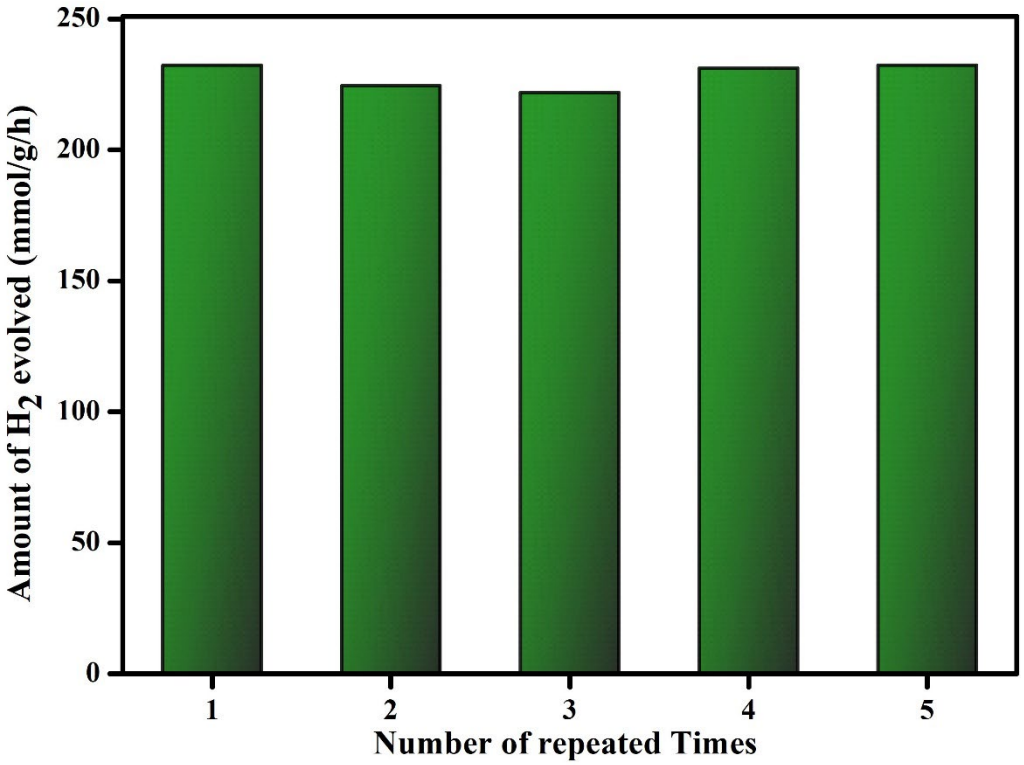

Figure S10: H_2 production results of optimized CdS/SnS_2-WS_2 (6 wt. % of SnS_2 and WS_2) nanostructures under sunlight irradiation for five repeated times.

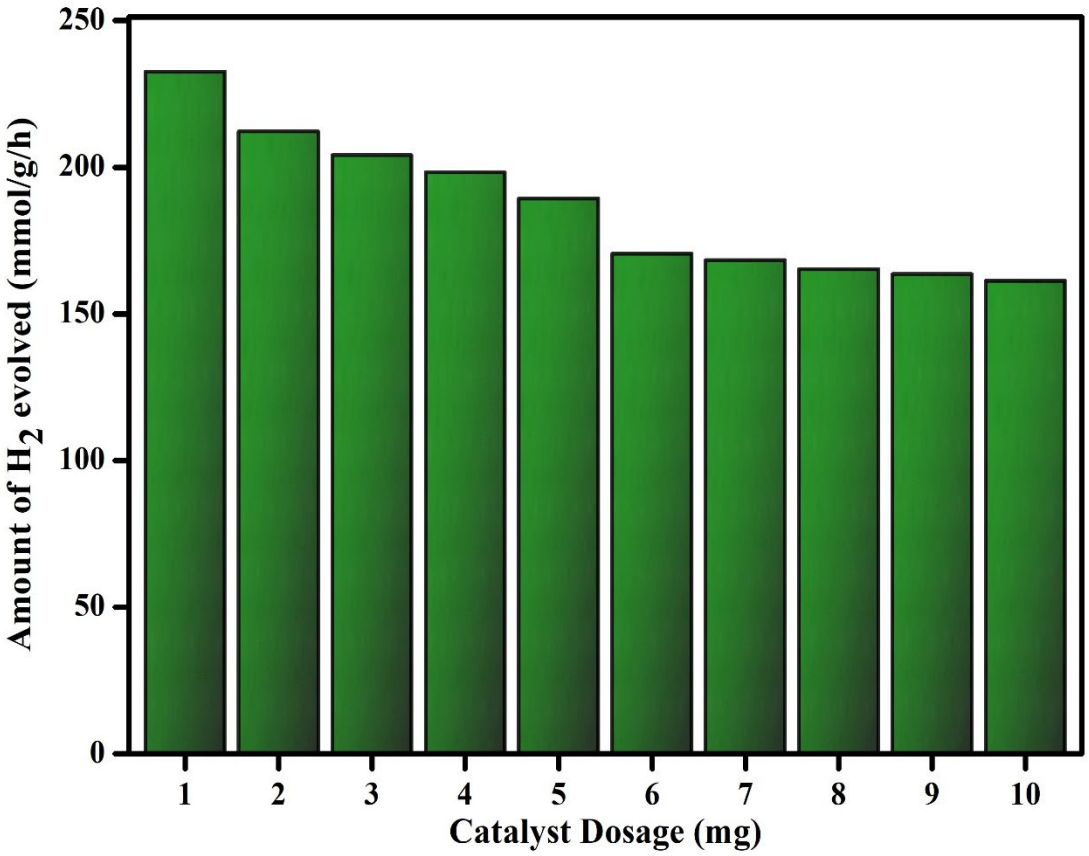

Figure S11: Amount of hydrogen evolution rate under sunlight irradiation using optimized CdS/ SnS_2-WS_2 nanostructures with different amount of catalyst loading (1-10 mg).

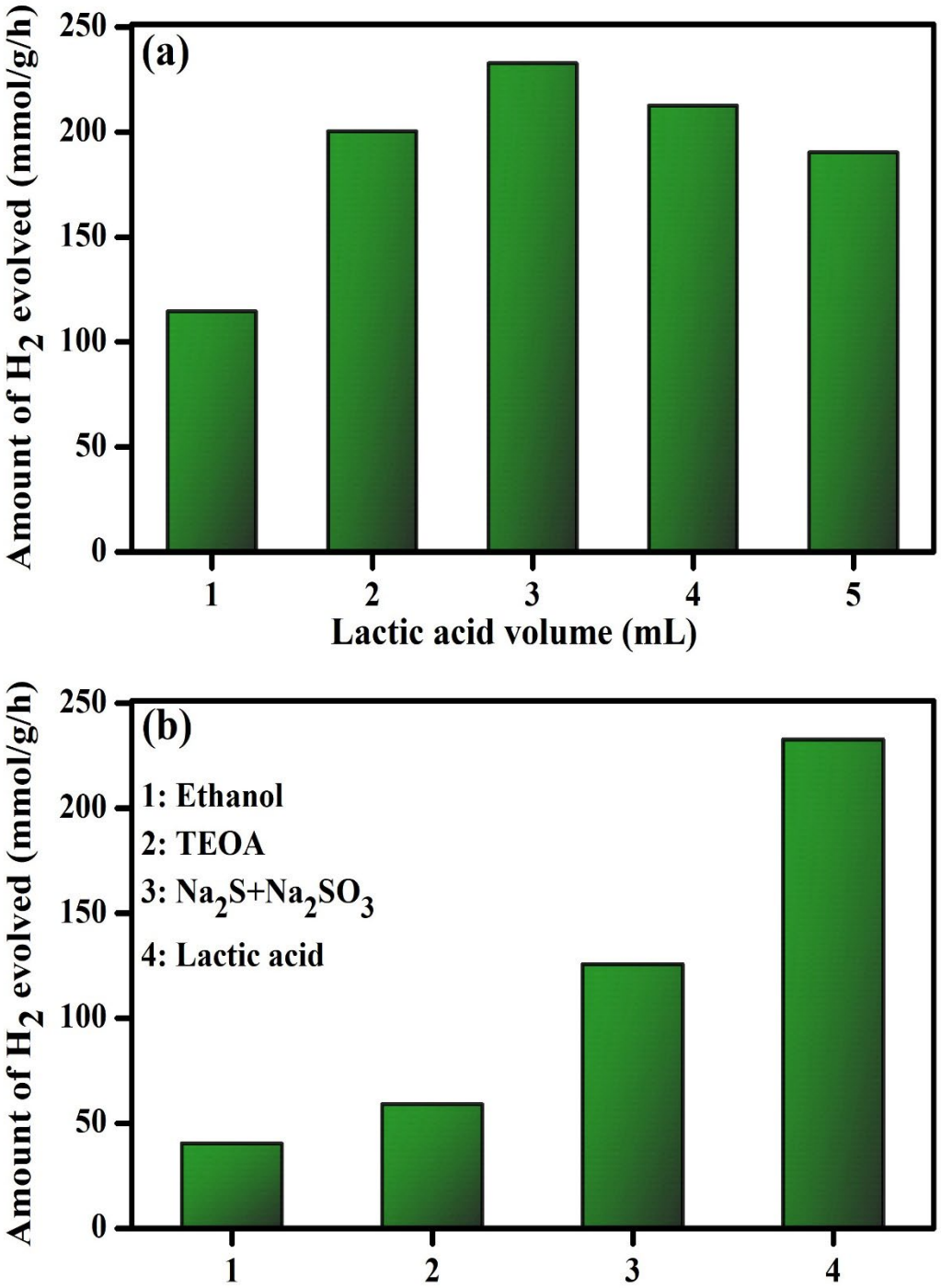

Figure S12: (a) Effect of amount of lactic acid solution on H_2 production rate of optimized CdS/SnS_2-WS_2 nanostructures (b) Amount of hydrogen evolution rate using optimized photocatalysts with different hole scavengers.

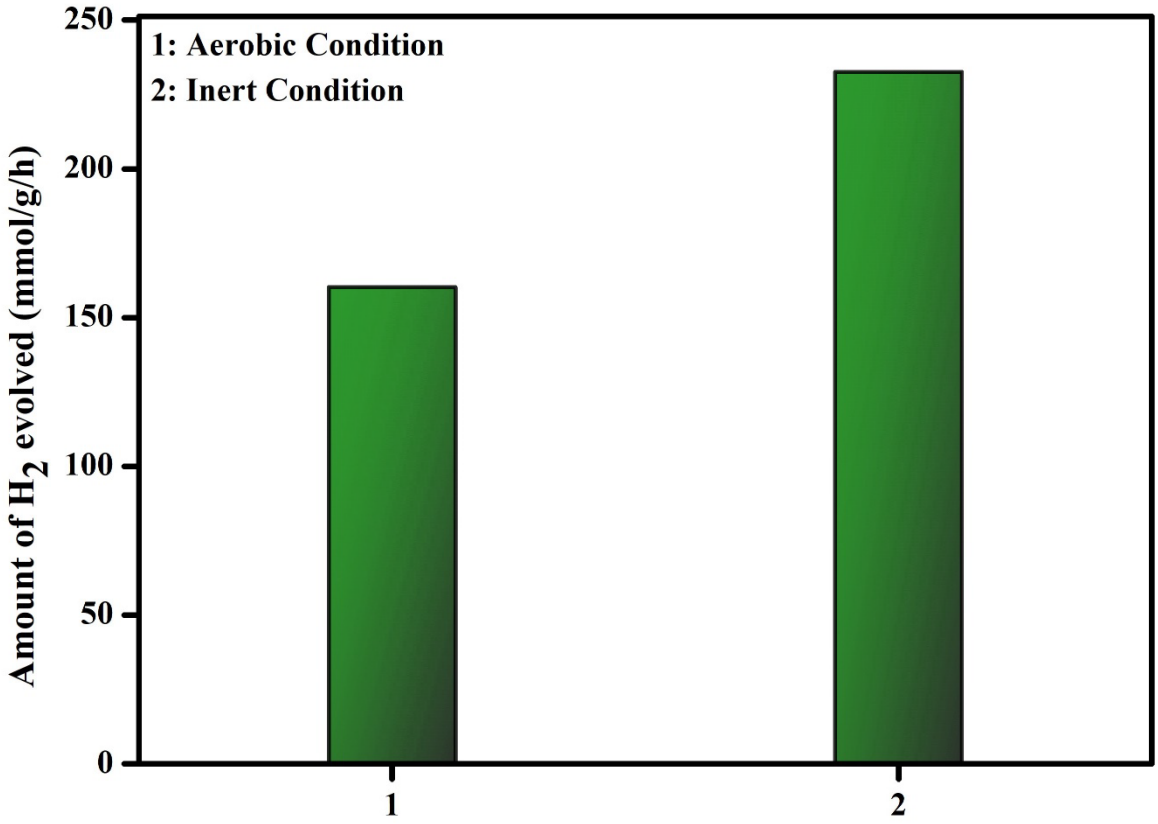

Figure S13: Amount of hydrogen evolved using optimized CdS/SnS_2-WS_2 photocatalyst under aerobic and inert condition.

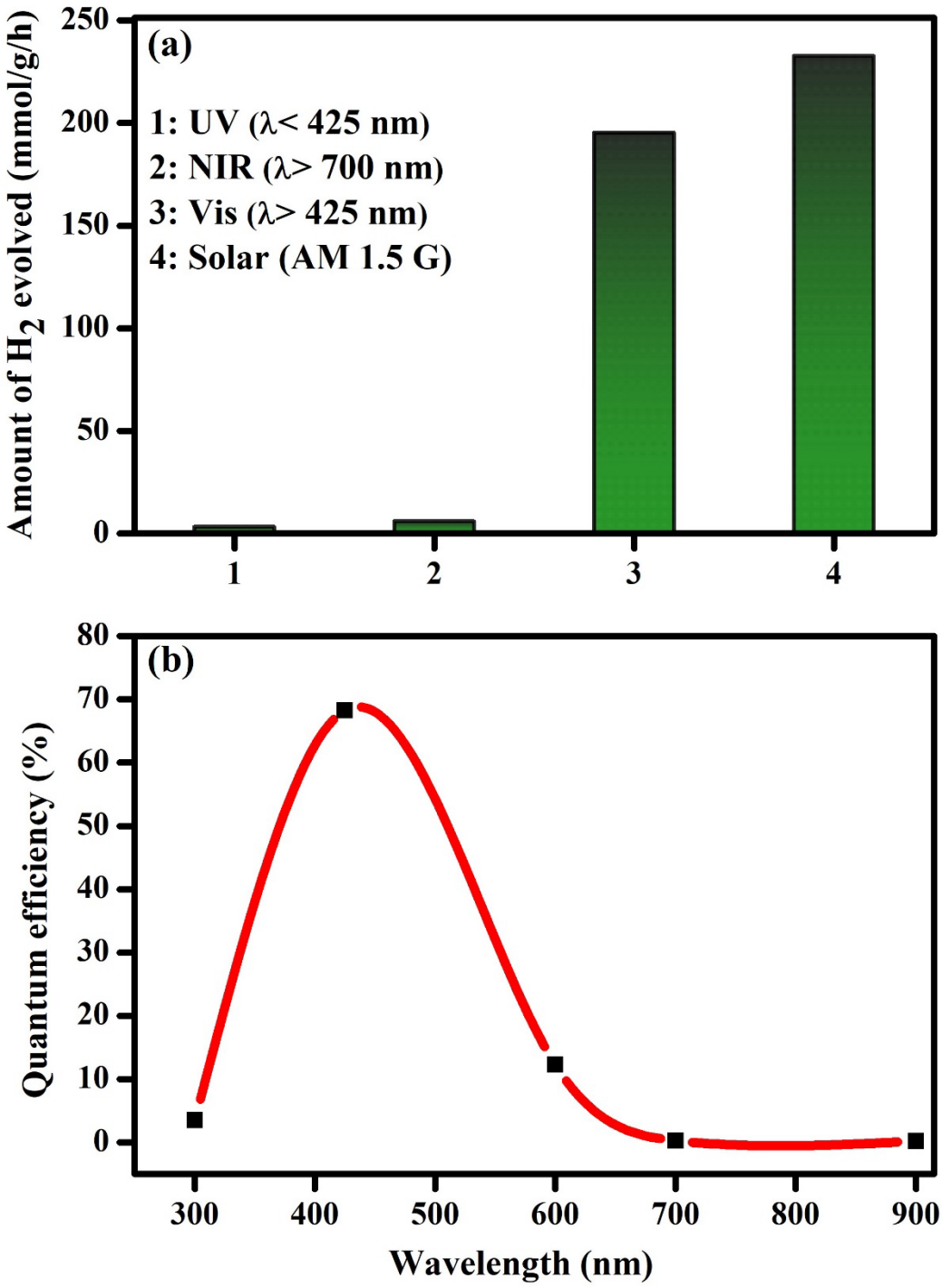

Figure S14: (a) Amount of hydrogen evolved for the optimized CdS/SnS_2-WS_2 photocatalyst at different wavelengths of light irradiation (b) QE of the optimized photocatalyst at different wavelength of light irradiation

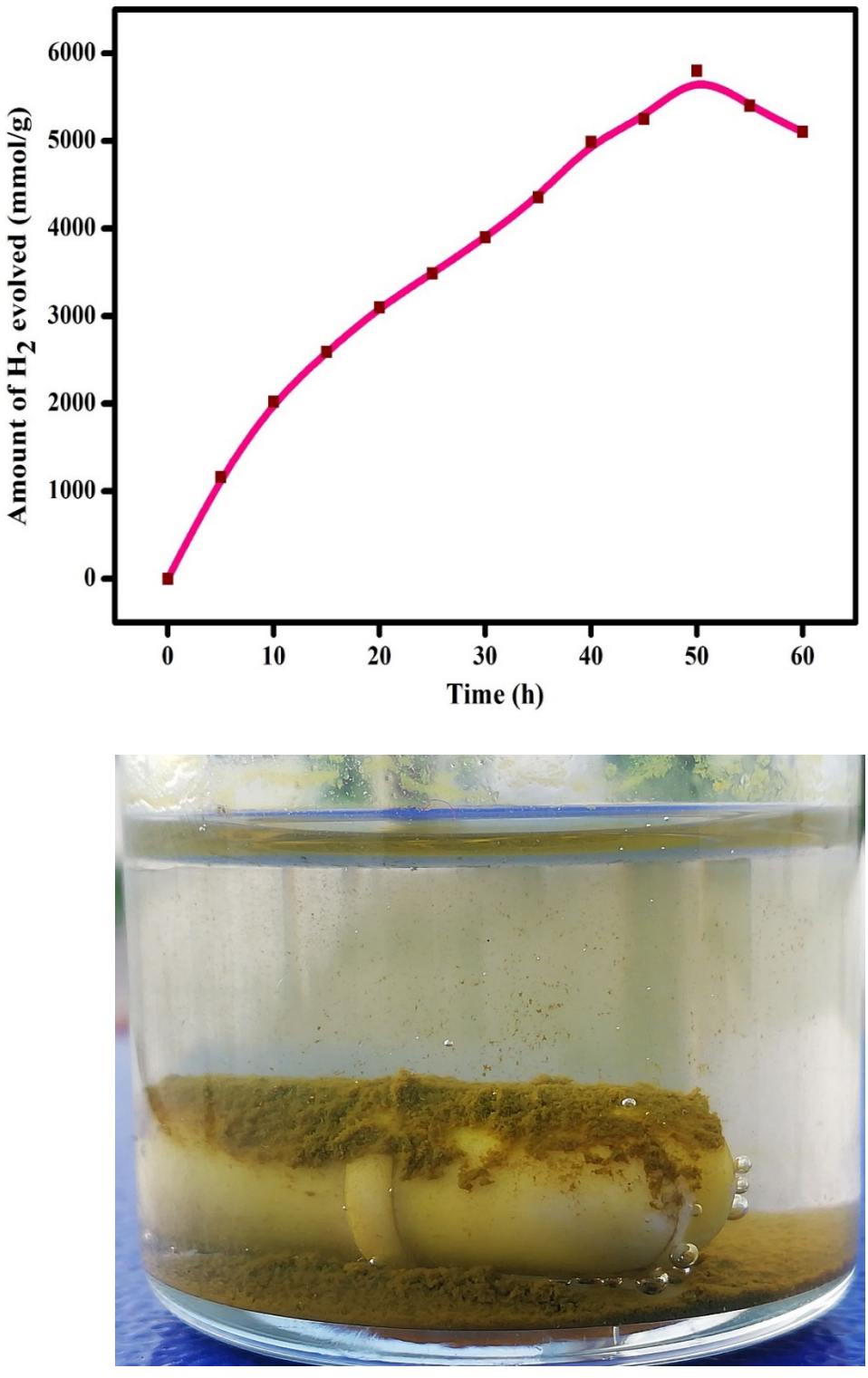

Figure S15: (a) Long-term stability of the optimized CdS/SnS_2-WS_2 nanocomposite under continuous photo-irradiation (b) Digital photograph of the hydrogen bubbles during the photocatalytic experiment

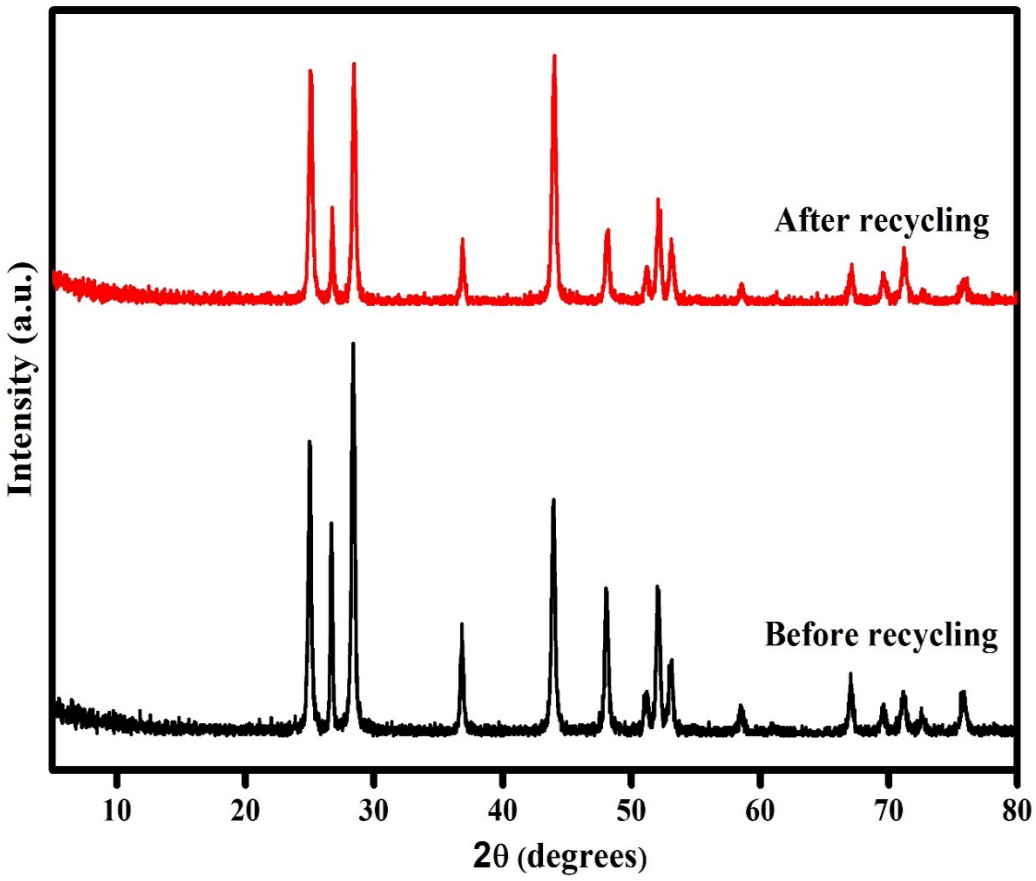

Figure S16: XRD patterns of before and after recycling of the optimized CdS/SnS_2-WS_2 photocatalysts

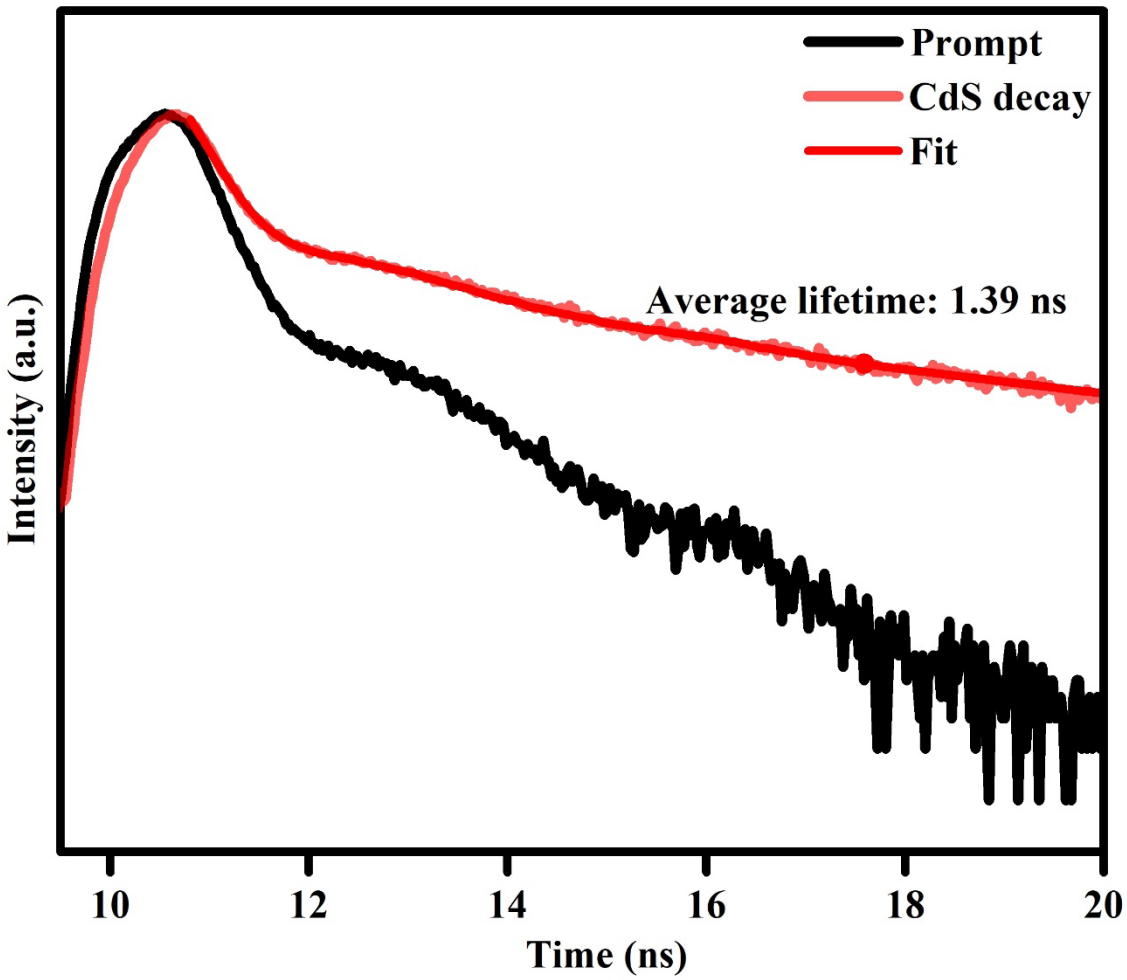

Figure S17: Time resolved PL spectra of CdS nanorods

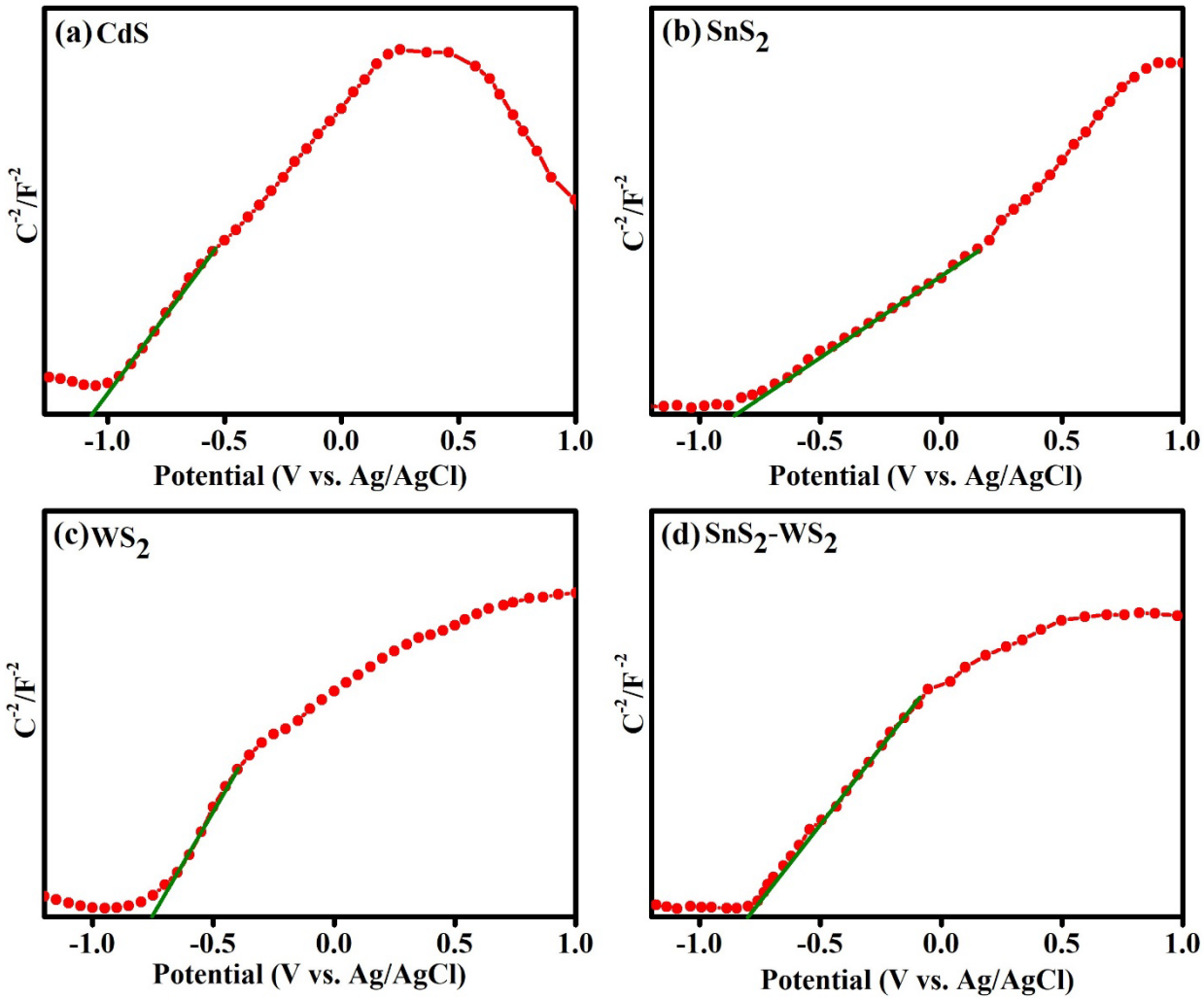

Figure S18: Mott-Schottky plots of (a) CdS, (b) SnS_2, (c) WS_2, and (d) SnS_2-WS_2 nanostructures

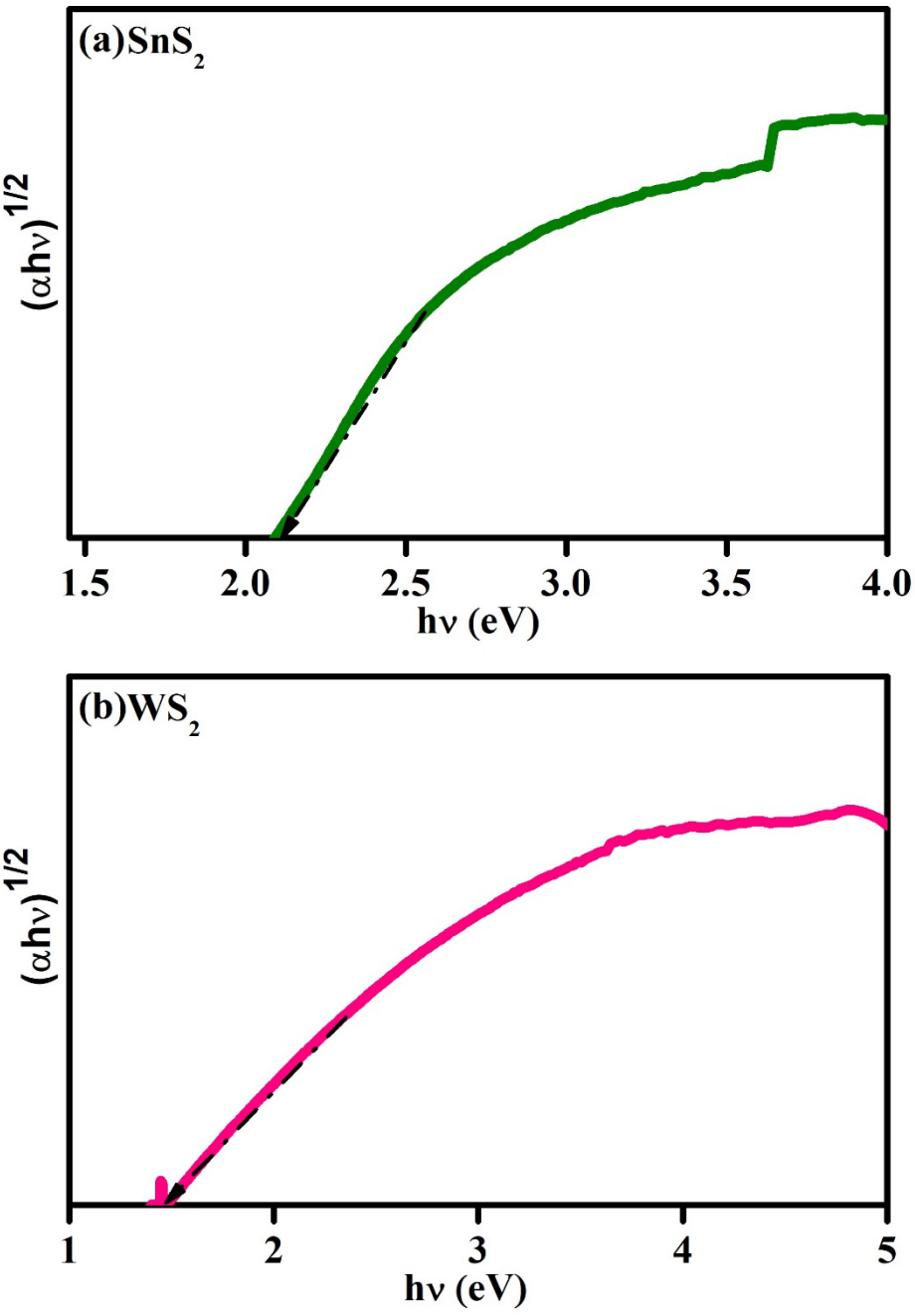

Figure S19: Tauc's plot of the (a) SnS_2 and (b) WS_2 nanostructures

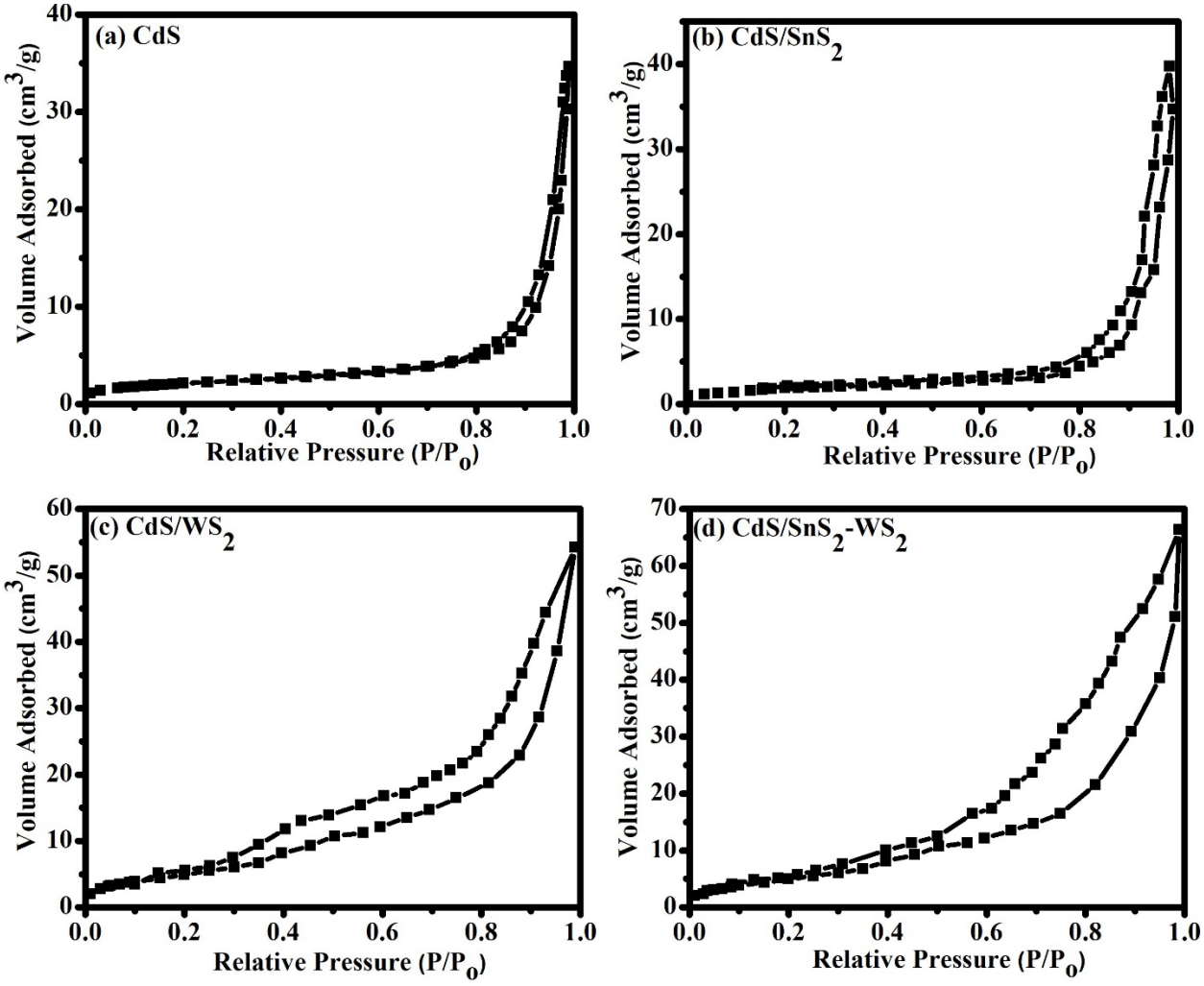

Figure S20: Nitrogen adsorption–desorption (BET) curves of (a) CdS, (b) CdS/SnS_2, (c) CdS/WS_2, and (d) CdS/SnS_2 -WS_2 nanostructures

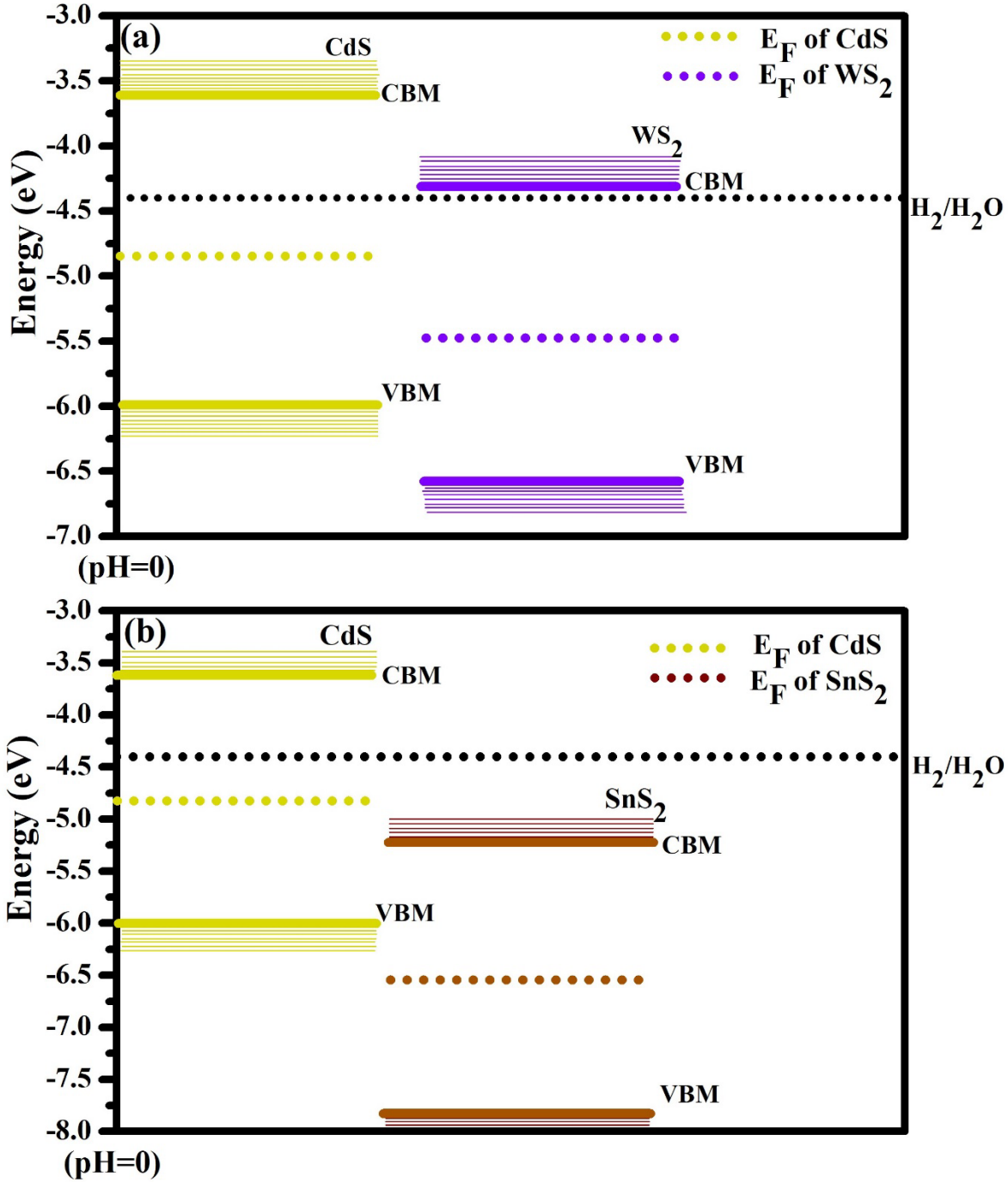

Figure S21: The alignment of band edge positions with respect to vacuum level for (a) CdS- WS_2, and (c) CdS-SnS_2 respectively. Water reduction potential is also shown for clarity.

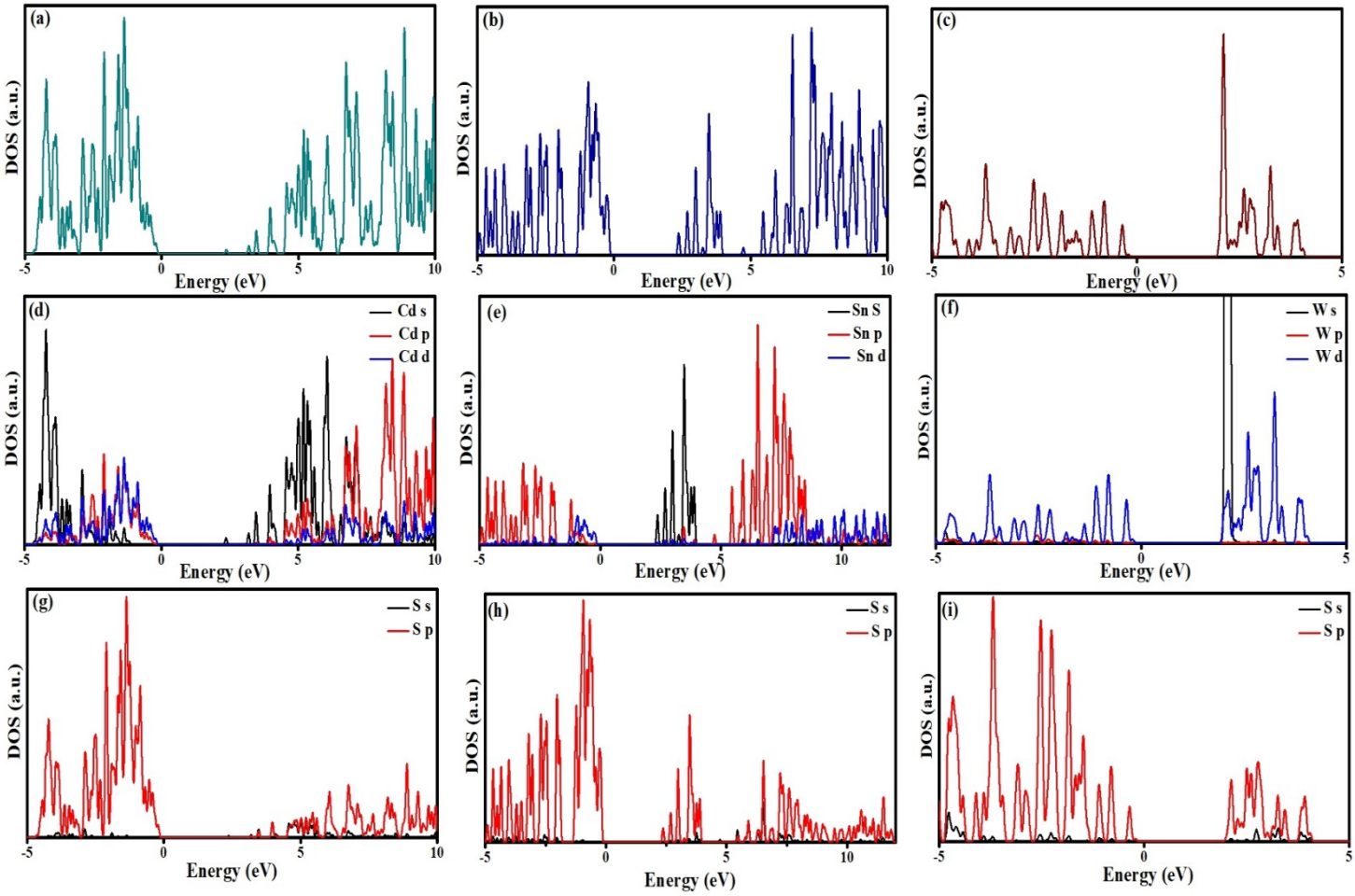

Figure S22: The HSE06 total electronic DOS of (a) CdS, (b) SnS_2, and (c) WS_2 respectively, (d-i) Partial DOS of Cd, Sn W and S respectively of CdS, SnS_2 and WS_2

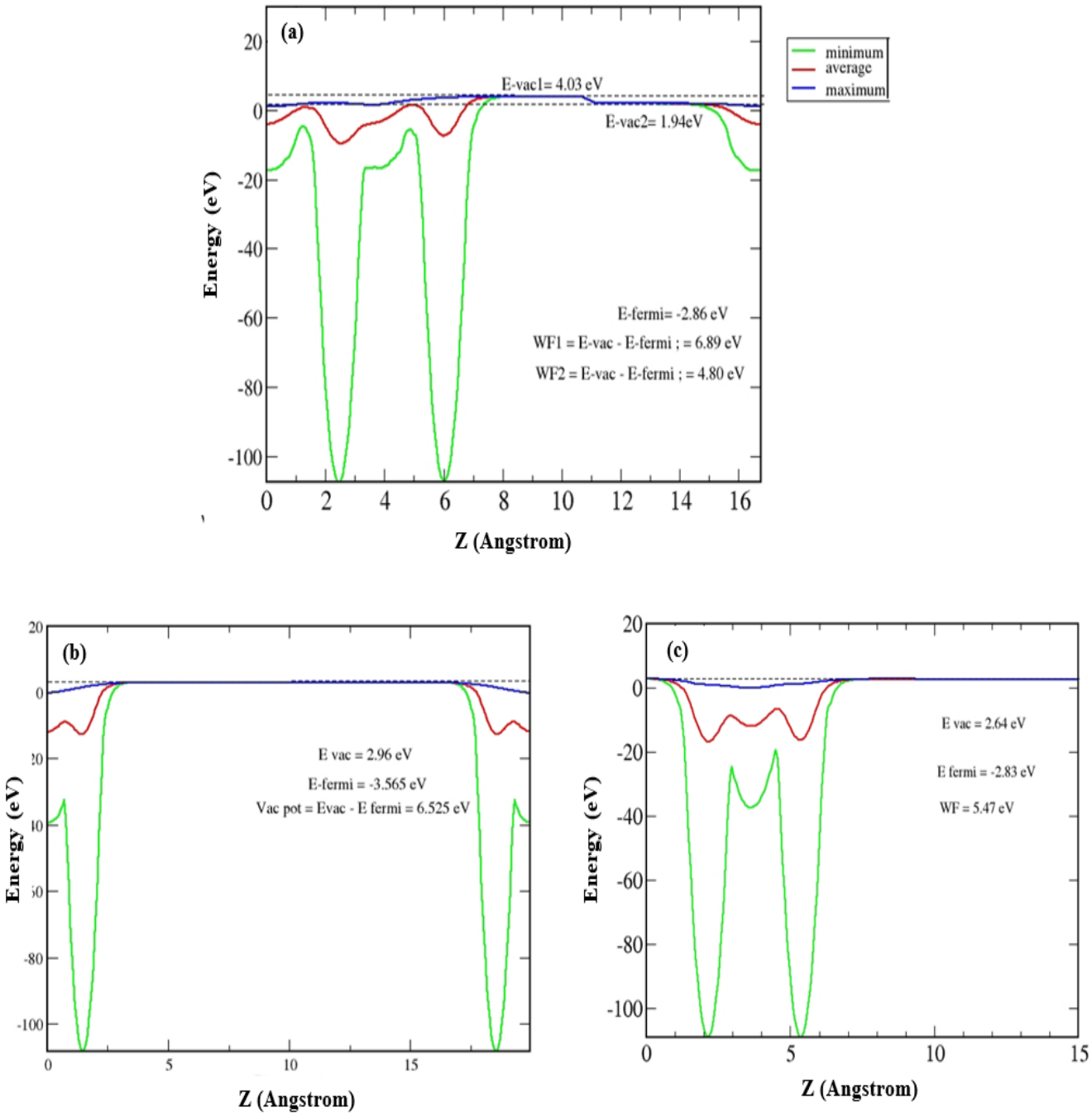

Figure S23: Electrostatic potential of (a) CdS, (b) WS_2, and (c) SnS_2 respectively

Table S1: Gibbs Free Energy data of CdS and SnS_2 and WS_2 nanostructures

Single point energy of H_2 molecule = -6.75839953

Single point energy of H atom alone in a box = -0.02814307

System	Total energy (eV)
WS_2	-94.86643012
WS_2-H-on W	-95.65210152
WS_2-H-on S	-96.26437643
SnS_2	-52.96152191
SnS_2- H- on Sn	-55.51471974
SnS_2-H-on-S	-55.49648451
CdS-NR- H	-275.27566582
CdS-NR- pristine	-272.71683803

Table S2. Comparison of Photocatalytic hydrogen evolution rate of CdS based nanocomposites mentioned in other literature with our obtained results

Photocatalyst	Scavenger	Light Source	H_2 Evolution Rate (mmol/g/h)	References
CdS/SnS_2-WS_2	Lactic Acid	Solar Simulator with AM 1.5 G Filter	232.45	Our work
CdS/WS_2	Lactic Acid	Xenon lamp (Asahi Spectra, LAX-C10) ($\lambda > 420$ nm)	14.1	[S4]
CdS/SnS_2 (Core Shell Heteronanostructure)	Lactic acid	150 W Xenon lamp ($\lambda >420$ nm)	35.65	[S5]
Nb_2O_5-SnS_2-CdS	Lactic acid	300-W Xe lamp	43.198	[S6]
WS_2/CdS	Lactic acid	350 W Xe lamp ($\lambda > 420$ nm)	61.1	[S7]
$NiSe_2$/CdS	50 mL Na_2S and Na_2SO_3	300 W Xe lamp ($\lambda > 420$ nm)	167.1	[S8]
B-Pt/CdS	Lactic Acid	350 W Xe arc lamp ($\lambda \geq 420$ nm)	1.49	[S9]
CdS/Co $(OH)_2$	Lactic acid	350 W Xe lamp ($\lambda > 420$ nm)	14.43	[S10]
CdS/MoS_2	Lactic Acid	Visible light ($\lambda>420$ nm)	91.2	[S11]
CdS@Ti_3C_2@CoO	No Scavenger	300 W Xe lamp ($\lambda \geq 420$ nm)	0.134	[S12]
CdS–Pd-Pt	Lactic acid	150 W Xenon lamp ($\lambda >420$ nm)	130.33	[S13]
CdS/Ti_3C_2	Lactic acid	300 W Xe lamp ($\lambda \geq 420$ nm)	2.407	[S14]
CdS/Co_3O_4	0.5 M Na_2S and Na_2SO_3	300 W Xe lamp ($\lambda > 420$ nm)	0.236	[S15]
CuS/CdS	0.35 Na_2S and 0.25 Na_2SO_3	300 W Xe lamp ($\lambda > 420$ nm)	0.28	[S16]
CdS/g-C_3N_4	0.1 M L-ascorbic acid	300 W Xe lamp ($\lambda > 420$ nm)	4.494	[S17]
CdS/ZnO-12	0.35 Na_2S and 0.25 Na_2SO_3	225 W Xenon arc lamp	22.12	[S18]

References

[S1] X. Shi, L. Mao, C. Dai, P. Yang, J. Zhang, F. Dong, L. Zheng, M. Fujitsuka, and H. Zheng, *J. Mater. Chem. A,* 2020, **8**, 13376–13384.

[S2] M. Harb, G, Jeantelot and J. M Basset, J. *Phys. Chem. C*., 2019, **123**, 28210–28218.

[S3] J. Greeley and J. K. Nørskov*, Surf. Sci*., 2007, **601**, 1590-1598.

[S4] K. Zhang, M. Fujitsuka, Y. Du, and T. Majima, *ACS Appl. Mater. Interfaces*, 2018, **10**, 20458–20466.

[S5] R. K. Chava, J. Y. Do, and M. Kang, *J. Mater. Chem. A*, 2019, **7**, 13614–13628.

[S6] K. K. Mandari, N. Son, S. Pandey, Y. S. Kim, G. A. K. M. Rafiqul Bari, and M. Kang, *J. Alloys Compd.*, 2020, **835**, 155399.

[S7] J. He, L. Chen, Z. Q. Yi, C. T. Au, and S. F. Yin, *Ind. Eng. Chem. Res.*, 2016, **55**, 8327–8333.

[S8] Z. Chen, H. Gong, Q. Liu, M. Song, and C. Huang, *ACS Sustainable Chem. Eng.,* 2019, **7**, 16720–16728.

[S9] J. Jin, J. Yu, G. Liu, and P. K. Wong, *J. Mater. Chem. A*, 2013, **1**, 10927–10934.

[S10] X. Zhou, J. Jin, X. Zhu, J. Huang, J. Yu, W. Y Wong, and W. K Wong, *J. Mater. Chem. A*, 2016, **4**, 5282–5287.

[S11] D. Ma, Q. Lu, E. Guo, F. Tao, and M. Wei, *Chemistry Select,* 2021, **6**, 2561–2568.

[S12] Z. Ai, K. Zhang, B. Chang, Y. Shao, L. Zhang, Y. Wu, and X. Hao, *Chem. Eng. J.*, 2020, **383**, 123130.

[S13] H. Park, D. A. Reddy, Y. Kim, S. Lee, R. Ma,T. K. Kim, *Chem. Eur. J.*, 2017, **23**, 13112-13119.

[S14] R. Xiao, C. Zhao, Z. Zou, Z. Chen, L. Tian, H. Xu, H. Tang, Q. Liu, Z. Lin, and X. Yang., *Appl. Catal. B Environ.,* 2020, **268**, 118382.

[S15] J. Yuan, J. Wen, Q. Gao, S. Chen, J. Li, X. Li and Y. Fang, *Dalt. Trans.,* 2015, **44**, 1680–

1689.

[S16] I. Vamvasakis, A. Trapali, J. Miao, B. Liu, and G. S. Armatas, Inorg. *Chem. Front.*, 2017, **4**, 433–441.

[S17] S. W Cao, Y. P. Yuan, J. Fang, M. M. Shahjamali, F. Y. C. Boey, J. Barber, S. C. J. Loo, and C. Xue, *Int. J. Hydrogen Energy,* 2012, **38**, 1258–1266.

[S18] D. Ma, J.W. Shi, Y. Zou, Z. Fan, X. Ji, and C. Niu, *ACS Appl. Mater. Interfaces*, 2017, **9**, 25377–25386.